Kinetics of Alkali Metal Ion Exchange into Nanotubular and Nanofibrous Titanates

Dmitry V. Bavykin* and Frank C. Walsh

Electrochemical Engineering Laboratory, Energy Technology Research Group, School of Engineering Sciences, University of Southampton, Highfield, Southampton SO17 1BJ, United Kingdom

Received: May 16, 2007; In Final Form: June 28, 2007

The kinetics of intercalation of Li^+, Na^+, K^+, and Cs^+ cations between the layers of titanate nanotubes and nanofibers have been studied in an aqueous suspension of nanotubes at 25 °C. The rate of intercalation was found to be similar for different cations and depended on the length of the nanotubes. The decrease in nanotube length resulted in a higher rate of ion exchange, indicating that the transport of cations in titanate nanotubes occurred probably along their length. In contrast, the transport of cations in titanate nanofibers probably dominated in the direction perpendicular to length. Correlations between the rate of intercalation and the crystal structure modification following intercalation have been established for nanotubular and nanofibrous titanates.

Introduction

Quasi one-dimensional metal oxide materials continue to attract much attention.[1,2] Nanostructured (especially nanotubular or nanofibrous) titanates are interesting due to their unusual physicochemical properties[3,4] and their potential use in energy applications including hydrogen storage[5] and lithium batteries.[6,7] The properties of open mesoporous morphology,[8] good ion exchange,[9] and nanometer scale of the materials could be utilized in applications where ionic transport is an essential part of the process. Such applications include advanced ion-exchange membranes for hydrogen fuel cells,[10] recovery of metals from waste solutions including control and management of radioactive wastes,[11] and materials for metal oxide semiconductor field effect transistors.[12] For successful applications, it is important to know the ion-exchange characteristics of nanostructured titanates.

For titanate nanotubes it has been shown[13] that exchangeable cations occupy positions between the titanate layers (inside the wall of multiwall nanotubes) as well as on the surface of the nanotubes. In solid nanofibers, the cations of alkali metals also occupy the interlayer spacing between (100) planes inside the fiber. The detailed mechanism of intercalation of cations into the crystal structure of titanate nanotubes or nanofibers and the factors affecting the regularities of cation intercalation are still unclear.

An improved understanding of the effect of the dimensions of nanostructured titanates on the kinetics of ion intercalation can provide an insight into the mechanism of transport of ions in these nanostructures. Such knowledge will help to determine the direction of ion movement through the crystal structure of titanates as well as facilitate control over the rate of ion exchange by alteration of the morphology of nanostructures.

In this work, the effect of titanate nanotube dimensions (length and diameter) on the dynamics of lithium intercalation from aqueous solution has been studied for the first time. The effect of the alkaline metal cation on the rate of the intercalation and the crystal structure of nanotubular lithium, sodium, potassium, and cesium titanates has been investigated. The transport of lithium ions in titanate nanotubes and nanofibers has been compared. The alteration of crystal structure during intercalation of alkaline ions into the titanate nanotubes and nanofibers has been correlated with the kinetics of intercalation allowing a discussion of the mechanism and direction of ionic diffusion in titanate nanocrystals.

Experimental Details

Reagents. Titanium dioxide (anatase, TiO_2), sodium hydroxide (NaOH), lithium hydroxide (LiOH), potassium hydroxide (KOH), cesium hydroxide (CsOH), sulfuric acid (H_2SO_4), and hydrochloric acid (HCl), pure grade, were obtained from Aldrich and used without further purification.

Preparation of Protonated Titanate Nanotubes and Nanofibers. The preparation of titanate nanotubes was based on the alkaline hydrothermal method proposed by Kasuga et al.[14] and further developed in our laboratories.[8] An amount of 25 g of titanium dioxide (anatase) was added to 300 cm^3 of 10 mol dm^{-3} NaOH solution in a PTFE beaker under vigorous stirring. The solution was placed in a PTFE-lined autoclave and heated for 22 h at 140 °C for the synthesis of nanotubes and at 170 °C for the preparation of nanofibers. The white, powdery titanates produced were thoroughly washed with water until the washing solution achieved pH 7. In order to convert nanostructured titanates into their protonated form, the powder was washed with excess of 0.1 mol dm^{-3} HCl for over 30 min until a stable pH value of 2, followed by water washing to pH 5. The sample was dried in air at 120 °C.

Measurement of the Kinetics of Ion Exchange. For measurements of alkaline ions intercalation into nanostructured titanates, 0.1 g of dry powder sample, in the protonated form, was placed in the beaker and 10 cm^3 of water was added. Under vigorous stirring, a chosen volume (x) of 1 mol dm^{-3} of base solution was then quickly added. The dynamics of pH change were recorded using a Corning 250 ion analyzer equipped with glass electrodes at 25 ± 1 °C. In order to record the protonation reaction, $x + 10$ μL of 1 mol dm^{-3} HCl was added and the pH was recorded with time. The ultrasonic treatment of an aqueous

* To whom correspondence should be addressed. Tel.: +44 2380598358. Fax: + 44 2380598754. E-mail: D.Bavykin@soton.ac.uk.

10.1021/jp073799a CCC: $37.00
Published on Web 09/18/2007

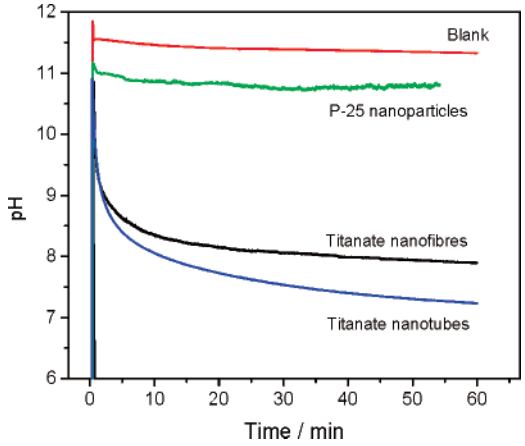

Figure 1. pH as a function of time following addition of 50 μL of 1 mol dm^{-3} LiOH to a suspension of 0.1 g of TiO_2 or titanate solid in 10 mL of water at 25 °C. Initial pH of water is ca. 4.5.

suspension of titanate powder was performed using a VWR ultrasonic bath (USC 300TH 80 W, 45 Hz) for controlled times.

Sample Characterization. The BET surface area and BJH pore distribution of the samples were measured, using nitrogen adsorption, on a Micromeritics ASAP 2010 instrument. TEM images were obtained using a JEOL 3010-TEM transmission electron microscope. The powder sample was "dry" deposited onto a copper grid covered with a perforated carbon film. SEM images were obtained with a JEOL 6500 FEG-SEM scanning electron microscope. The sample was dispersed in water, deposited on flat silicon wafers, then dried at room temperature. XRD patterns were recorded using a Bruker AXS D8 Discoverer X-ray diffractometer, with Ni-filtered Cu Kα radiation (λ = 0.154 nm) and a graphite monochromator, in the 2θ range of 5−40°.

Results and Discussion

Exchange of Lithium Ions. Nanostructured TiO_2 is one of the possible candidate materials for the cathode coatings of lithium batteries.[6,7,15] Recently, nanotubular[16,17] and nanofibrous[18,19] titanates have also demonstrated a promising performance as positive electrode materials for lithium batteries. An essential step in the use of nanostructured TiO_2 materials is the intercalation of lithium atoms. The optimization of efficiency, capacity retention after cycling, and kinetics of charge/discharge in lithium batteries requires an understanding of the mechanism and kinetic characteristics of lithium ion intercalation into nanotubular or nanofibrous titanates.

Nanostructured titanates produced by alkaline hydrothermal treatment of TiO_2 are characterized by an open, mesoporous morphology, high specific surface area, and good ion-exchange properties. The crystal structure of protonated nanostructured titanates is still disputed. Titanate nanotubes include $H_2Ti_3O_7$,[20] $H_2Ti_2O_4(OH)_2$,[21] $H_2Ti_4O_9{\cdot}H_2O$,[22] and TiO_2-B,[23] whereas titanate nanofibers can be represented as $H_2Ti_6O_{13}$[24] and $H_2Ti_8O_{17}$.[25] The generalized formula of these protonated titanates can be represented as $H_2Ti_nO_{2n+1}{\cdot}xH_2O$. The solubility of titanate nanotubes in aqueous solution is very low,[26] and the proton exchange with alkali metal cations can then be represented by

$$xM^+ + H_2Ti_nO_{2n+1} \leftrightarrow M_xH_{2-x}Ti_nO_{2n+1} + xH^+ \qquad (1)$$

where M^+ is the alkaline metal cation. The ion-exchange reaction 1 is reversible, and the value of x is expected to depend on pH, M^+ concentration, and temperature.

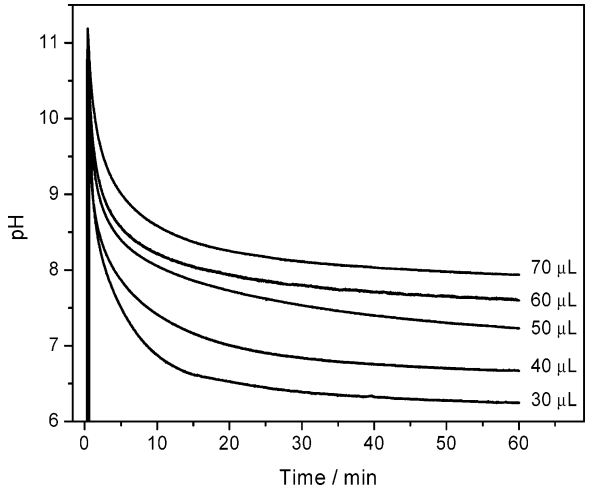

Figure 2. pH changes with time, following addition of controlled volumes of 1 mol dm^{-3} LiOH(aq) to a suspension of 0.1 g of protonated titanate nanotubes in 10 mL of water at 25 °C.

Figure 1 shows the dynamics of pH change in an aqueous suspension of nanostructured titanate and titania after addition of aqueous LiOH. For the blank solution of pure water, the addition of LiOH results in a very rapid increase of pH up to a value of 11.5 and an almost constant value within 60 min of measurements. The small decrease of pH is attributable to reaction with atmospheric CO_2 forming lithium carbonate. The addition of the same amount of LiOH to a suspension of TiO_2 nanoparticles (Degussa P-25), which are characterized by spheroidal particles of ca. 20 nm diameter, results in a rapid increase of pH up to 11 followed by an insignificant drop. In contrast, the addition of the same amount of LiOH to a suspension of titanates nanotubes and nanofibers results in an initial, rapid rise of pH until approximately pH 11, followed by a slow decrease of pH to the values 7.3 and 8.1, respectively. The characteristic time of the pH decrease is in the range of several tens of minutes.

The specific surface area of Degussa P-25 (ca. 50 m^2 g^{-1}) is lower than that of titanate nanotubes[8] (ca. 200 m^2 g^{-1}) but higher than the value for titanate nanofibers (ca. 20 m^2 g^{-1}). Thus, such insignificant drop of pH after addition of alkali to P-25 cannot be explained by small surface area. Such a high amplitude of the pH variations in the case of nanostructured titanates can be explained by the leaching the protons from the crystal structure of protonated titanates, which arises from the substitution of protons by lithium cations as shown in reaction 1. The dynamics of the pH change reflect the kinetic regularities of the ion exchange in nanotubular and nanofibrous titanates.

Figure 2 shows the dynamics of pH change after addition of various amounts of lithium hydroxide to the aqueous suspension of protonated titanate nanotubes at 25 °C. The increase of the volume of the added LiOH results in an increase of the steady-state pH. The characteristic time of the pH decay, however, does not change significantly suggesting that the limiting stage of the process probably does not depend on the concentration of Li^+ and H^+ in the bulk solution.

Titanate nanotubes are fragile structures which usually fracture along their length during mechanical treatment by, e.g., ultrasound.[8] This allows the average length of nanotubes to be adjusted, without a change in the average diameter, using the ultrasound treatment of aqueous suspension of sample. Figure 3 shows the SEM images and histograms of nanotubes length

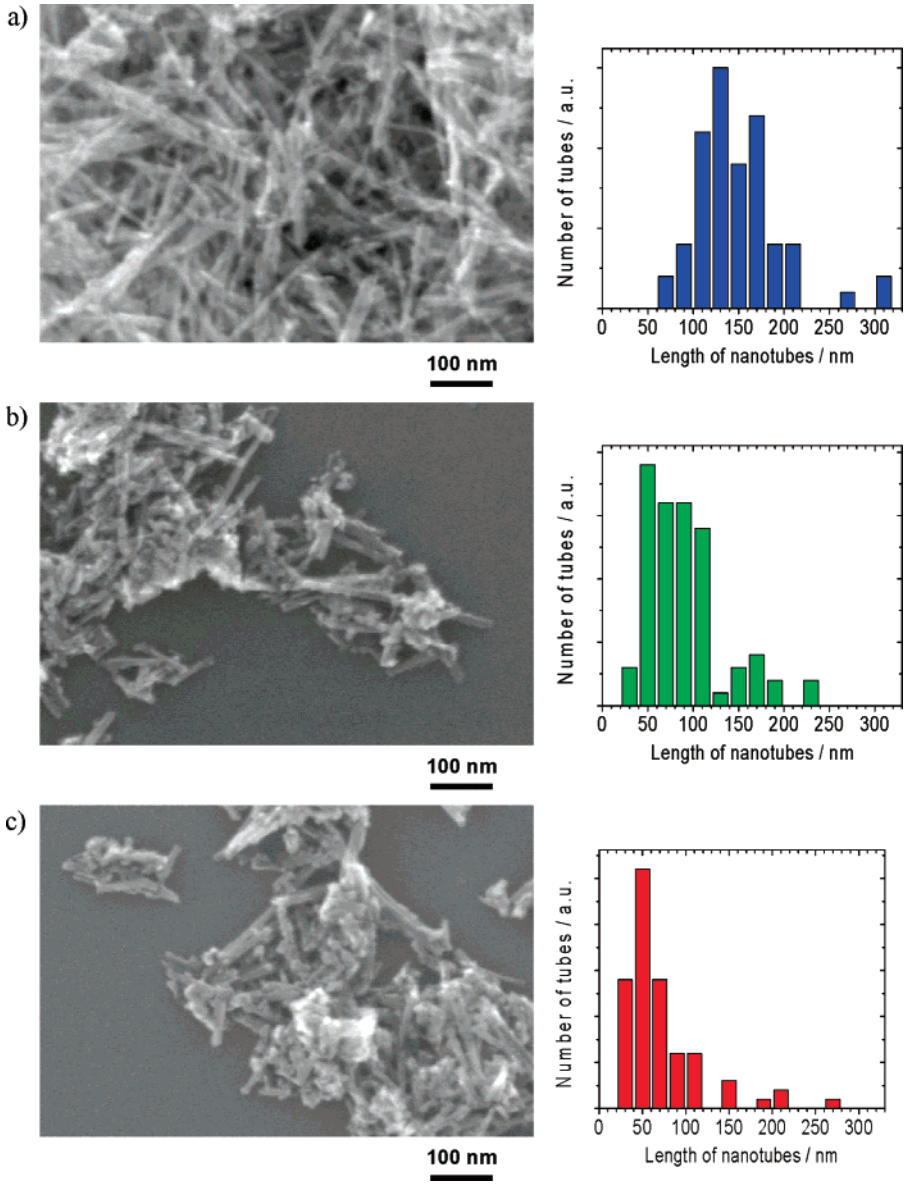

Figure 3. SEM images and histograms of length distributions of titanate nanotubes treated with ultrasound in aqueous suspension for controlled time: (a) initial nanotubes, (b) after 0.5 h, and (c) after 3 h. The histograms were constructed by measuring the number of nanotubes of a particular length from SEM images.

distribution for titanate nanotubes treated by ultrasound for different times. The longer time of ultrasonic treatment the shorter the average length of the nanotubes.

The length of nanotubes was found to affect the kinetics of ion exchange, and the decrease of the average nanotubes length could facilitate ion exchange. Figure 4 shows the kinetic curves of pH decay following addition of LiOH to a suspension of the nanotubes having selected average lengths. For the shortest nanotubes (having an average length ca. 50 nm), the characteristic time of the ion exchange was shorter than that for long nanotubes, suggesting that the diffusion of ions along the length of the tube could be the rate-limiting step. The value of steady-state pH was the same for all three samples, suggesting that the long and short tubes have similar numbers of ion-exchange sites. In contrast, the variation in the average (internal) diameter of nanotubes in the range from 3 to 8 nm did not affect the kinetics of ion exchange within the experimental error. (These data are not shown here.)

Simulation of Kinetics. The pH of the solution is related to the concentration of protons via logarithmic law ($pH = -\log([H^+])$. The typical kinetic curve of proton concentration growth in the suspension of protonated titanate nanotubes after addition of LiOH had the S-shape shown in Figure 5. The curve demonstrated a short induction period followed by monotonic growth and saturation. The release of protons from the titanate nanotubes to the bulk solution can be illustrated using the following sequence of processes:

$$Li^+_{bulk} \rightarrow Li^+_{surface} \quad (2.1)$$

$$Li^+_{surface} \rightarrow Li^+_{intercalate} \quad (2.2)$$

$$Li^+_{intercalate} + H_2Ti_nO_{2n+1} \rightarrow LiHTi_nO_{2n+1} + H^+_{intercalate} \quad (2.3)$$

$$H^+_{intercalate} \rightarrow H^+_{surface} \quad (2.4)$$

$$H^+_{surface} \rightarrow H^+_{bulk} \quad (2.5)$$

The resultant process corresponds to reaction 1 with Li^+ as the intercalating ion and $x = 1$. Step 2.1 represents the adsorption of lithium ions from bulk solution onto the surface of nanotubes;

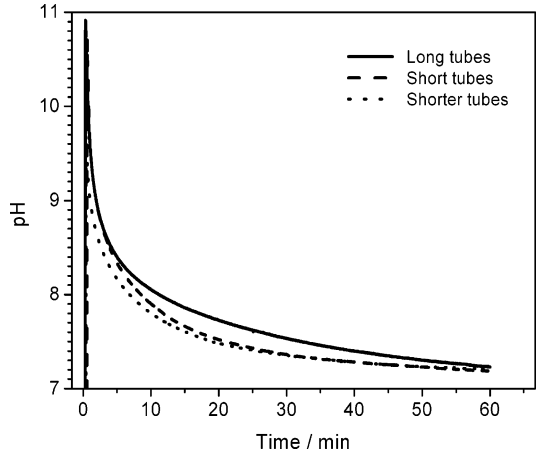

Figure 4. pH decay after addition of 50 μL of 1 mol dm^{-3} LiOH to a suspension of 0.1 g of protonated titanate nanotubes having various lengths in 10 mL of water at 25 °C. The length of tubes was tuned by ultrasonic treatment. "Long" tubes corresponds to the initial nanotubes, "short" tubes were obtained after 0.5 h, and "shortest" ones after 3 h of ultrasonic treatment.

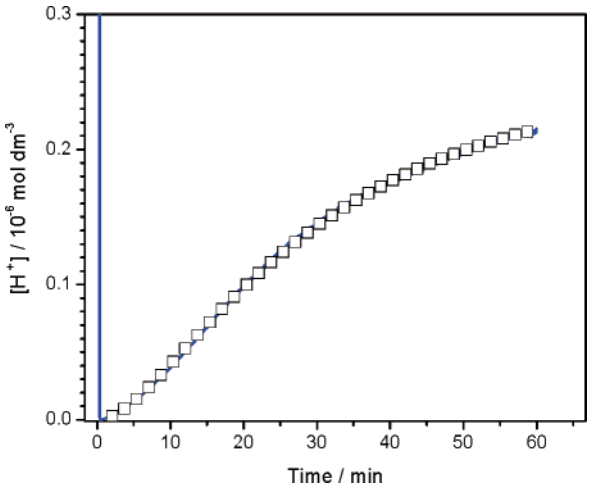

Figure 5. Proton concentration growth with time (□) after addition of 40 mL of 1 mol dm^{-3} LiOH to a suspension of 0.1 g of protonated titanate nanotubes in 10 mL of water at 25 °C. The line was fitted using eq 4.

step 2.2 is the transport of lithium ions inside the crystal to the centers of ion exchange. The process 2.3 is the chemical reaction of ion exchange, which occurs inside the crystal. Steps 2.4 and 2.5 represent the reverse transport of protons from the crystal to the surface then to the bulk solution. The fact that the length of nanotubes affects the rate of overall process may indicate that the transport of lithium ions and protons between the layers inside the wall of nanotubes are the rate-limiting steps. Therefore, the above scheme can then be simplified by exclusion of fast processes in two consecutive stages, namely, diffusion of lithium ions (A to B) and diffusion of protons (B to C) inside the wall of nanotubes.

$$\mathrm{A} \xrightarrow{k_1} \mathrm{B} \xrightarrow{k_2} \mathrm{C} \qquad (3)$$

where k_1 and k_2 are reaction constants. Scheme 3 is deliberately oversimplified in order to demonstrate the appearance of an induction time in the kinetic curve of proton concentration growth. More detailed treatments should consider the transformation from A to B not as a chemical reaction but rather as a diffusion process inside the nanotube. The analytical solution

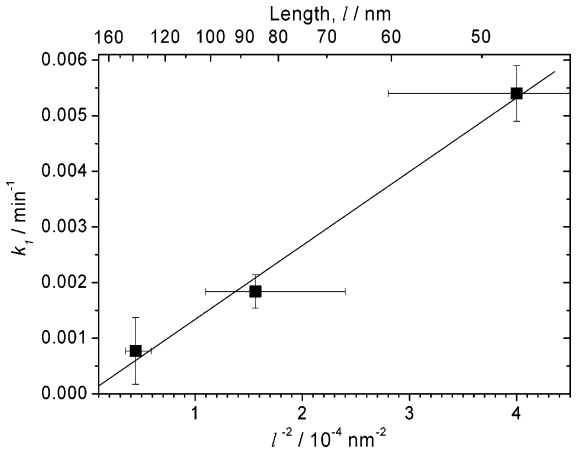

Figure 6. Rate of lithium ion intercalation (k_1) as a function of the square reciprocal length of nanotubes (l). The value of k_1 was determined by fitting eq 4 to the experimental kinetic curve of proton concentration growth. The value of l was determined as the average length of nanotubes from Figure 3 histograms.

for accumulation of C from the scheme 3 using acting mass law has the form[27]

$$C(t) = \frac{A_0}{k_2 - k_1}(k_2(1 - \mathrm{e}^{-k_1 t}) - k_1(1 - \mathrm{e}^{-k_2 t})) \qquad (4)$$

where A_0 is the infinity concentration of protons, while k_1 and k_2 are parameters characterizing the diffusion of lithium ions and protons inside the nanotubes, respectively.

Equation 4 is fitted to the experimental kinetic curve of proton concentration growth in Figure 5. The proposed scheme 3 is in agreement with experimental kinetics and allows us to explain the reasons of the induction period in the kinetic curve. The growth of proton concentration in suspension after addition of strong LiOH is due to leaching of protons from the solid nanotubes, which occurs due to the ion exchange with lithium cations diffused inside the nanotubes. At zero time, the concentration of lithium ions inside the nanotubes and the rate of the proton leaching are both equal to zero. As soon as lithium ions diffuse into the nanotubes, the reverse leaching of protons occurs after an induction time.

Although the mechanistic scheme 3 does not exactly correspond to the discussed process of diffusion of ions in solid materials, a general solution for diffusion in a cylinder[28] can be used to relate the reaction constant k_1 and a diffusion coefficient:

$$k_1 \sim \frac{D_{\mathrm{Li}}}{l^2} \qquad (5)$$

where D_{Li} is the diffusion coefficient of lithium ions inside the titanate nanotubes and l is the nanotube length.

In Figure 6, the k_1 reaction constant as a function of the square reciprocal length of nanotubes is shown. The values of k_1 were obtained by fitting experimental kinetic curves describing proton concentration growth (see Figure 4) for nanotubes having different lengths to eq 4. The values of nanotube length were determined as an average length taken from a histogram (see Figure 3). The determined values of k_1 and l are consistent with eq 5, indicating that the transport of lithium ions in titanate nanotubes probably occurs along the length of the nanotube. The value of the diffusion coefficient can be estimated as an order of magnitude of 10^{-11} cm^2 s^{-1}, which is much smaller than the self-diffusion coefficient of cesium ions in zeolite but

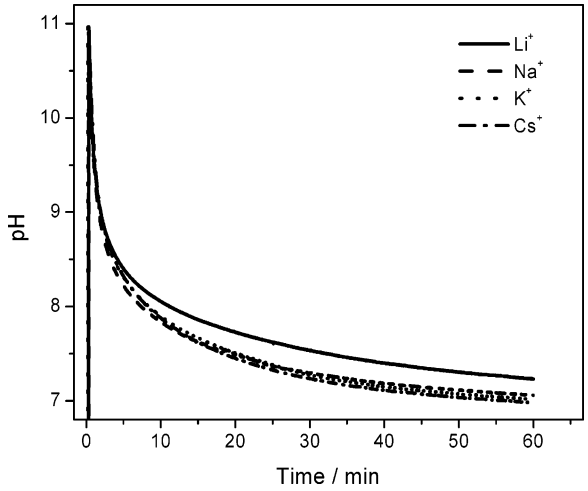

Figure 7. pH decay following addition of 50 μL of 1 mol dm^{-3} solution of alkali metal hydroxide to a suspension of 0.1 g of protonated titanate nanotubes in 10 mL of water at 25 °C.

a similar order of magnitude to that in cancrinite.[29] Similar values of diffusion coefficient were also observed for zirconium thiophophates.[30] For a more accurate determination of the diffusion coefficient, an improved model for forward and reverse diffusion of ions in cylindrical particles is needed.

Exchange of Alkaline Metal Cations. The diffusion of ions of alkaline metals inside nanotubes occurs between the titanate layers, which are characterized by a zigzag structure and ca. 0.72 nm average spacing. The sizes of the ions of alkaline metal in aqueous solution are smaller and have the following ionic diameters Li^+ (0.09 nm), Na^+ (0.116 nm), K^+(0.152 nm), Cs^+ (0.181 nm) for a coordination number of 6.[31] The size of the alkali metal ions would be expected to affect the rate of ions intercalation into the crystal structure of titanate nanotubes. A knowledge of this effect could facilitate the use of nanostructured titanates for separation of metal ions.

Figure 7 shows the kinetic curve for pH decay in a suspension of titanate nanotubes after addition of various alkali metal hydroxides. The pH decay reflects the rate of alkali metal ion intercalation inside the walls of nanotubes. Despite the differences in the size of alkali metal cations, the apparent rate of the intercalation is very similar for all of the ions studied. This unusual result of the absence of selectivity of titanate nanotubes in terms of alkali metal transport is consistent with the observation of crystal structure alterations after substitution of protons by alkali metal cations in nanotubular titanates.

In Figure 8, the XRD patterns of nanotubular titanate of alkali metals including lithium, sodium, potassium, and cesium are shown. The nanotubular titanates of alkali metals were prepared by ion exchange of the protonated form of titanate nanotubes in the excess, aqueous solution of alkali metal hydroxide for 24 h at 25 °C, followed by washing with water and drying at 120 °C. As far as the XRD pattern of titanate nanotubes is concerned, the characteristic reflection at small angles is usually associated with diffraction from the (200) plane, which is correlated with the spacing between the layers in the wall of nanotubes where transport of ions occurs. Any variations of this spacing as well as any distortion of the layered structure can be easily detected by the shift or disappearance of this characteristic reflection in XRD pattern. In the case of substitution of protons by alkali metal ions the characteristic reflection shifts toward smaller angles from ca. 10° (Figure 8 a) to ca. 7.5° (Figure 8 b−e). This corresponds to an increase of

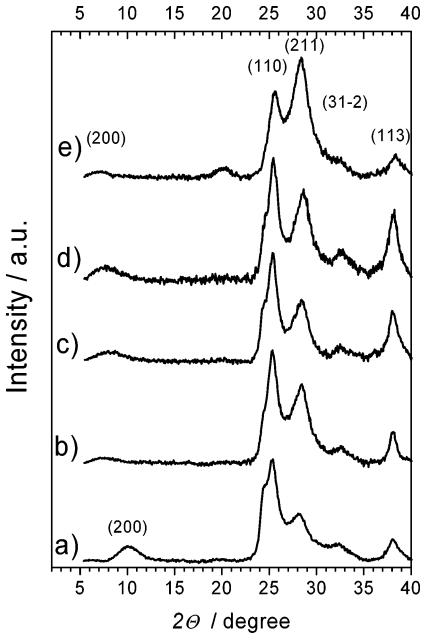

Figure 8. Powder XRD patterns of titanate nanotubes which have been ion-exchanged with different alkaline metal cations: (a) H^+, (b) Li^+, (c) Na^+, (d) K^+, and (e) Cs^+.

interplanar distance d_{200} from 0.88 to 1.18 nm, equivalent to an increase in the unit cell parameter, a, by almost 34%. Surprisingly, the interplanar distance d_{200} is almost the same for all nanotubular titanates studied and only the protonated form of the titanate nanotubes has a reduced value of the unit cell parameter, a. Such a similarity in the interlayer distances in nanotubular titanates of alkali metal was previously observed using high-resolution TEM (HRTEM) imaging[13] and is consistent with the similarity of the kinetic characteristics of ion exchange of protons to cations of alkali metals (Li^+, Na^+, K^+, and Cs^+) in titanate nanotubes.

TEM images also confirmed an increase of interlayer spacing in the wall of titanate nanotubes after substitution of protons by cesium ions (see Figure 9). According to microscopy data, the value of interlayer distance is approximately 0.72 nm for the proton form of nanotubes and ca. 0.91 for the cesium form of nanotubes, which is approximately a 26% increase.

The substitution of protons by alkaline metal cations in titanate nanotubes also results in a change in the ratio between the relative intensities of (110) and (211) reflections (see Figure 8). A similar tendency has also been observed elsewhere[32,33] and may be associated with different lattice distortions induced by alkali cations.

Nanofibers and the Effect of Fiber Length. Nanofibrous titanate nanostructures demonstrate similar ion-exchange properties to titanate nanotubes. Although the amount of ion-exchangeable centers in nanofibers is less than in nanotubes, the characteristic time of ion exchange between protons and lithium ion from aqueous solution is of the same order of magnitude (see Figure 1). The ultrasonic treatment of an aqueous suspension titanate nanofibers results in breaking of the structure along their length and splitting of the nanofibers, as shown in Figure 10, parts a and b, where SEM images of initial nanofibers and nanofibers after ultrasound treatment are presented. After such mechanical treatment, the average length and thickness of the fibers are reduced. Such a change in the dimensions of nanofibers results in facilitation of ion exchange without a change in its extent (see Figure 11) confirming that the ion transport inside nanofibers is a rate-limiting stage.

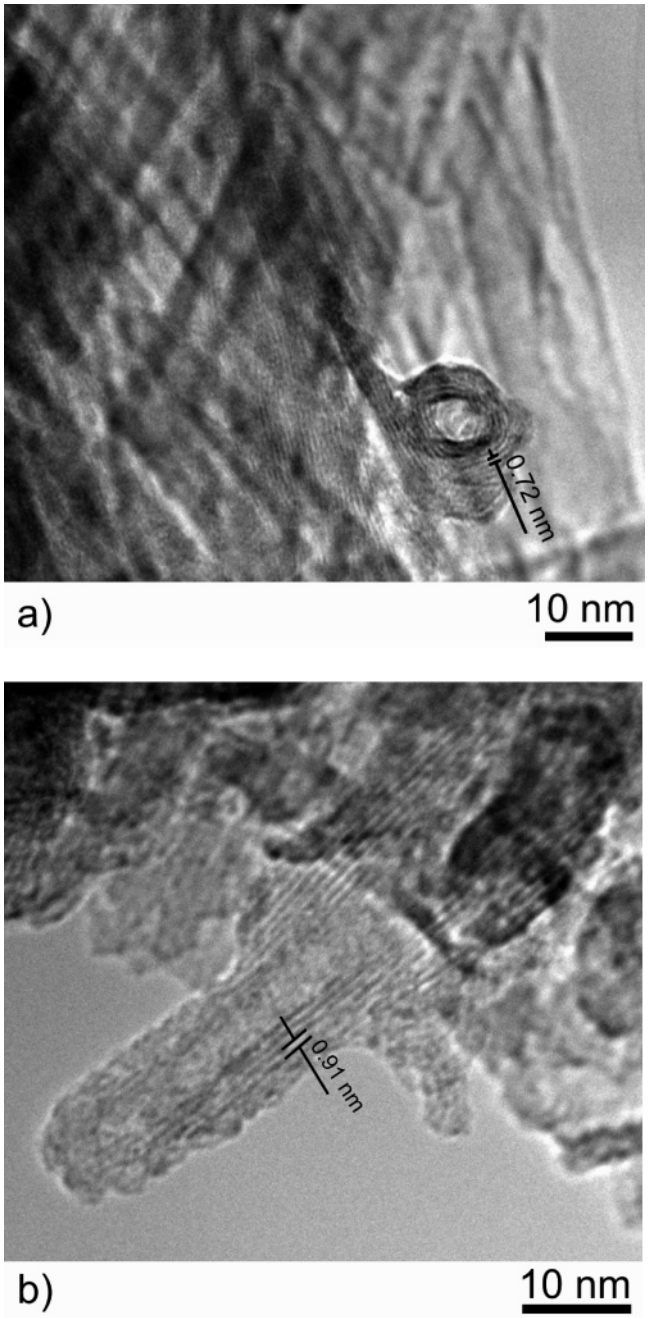

Figure 9. TEM images of titanate nanotubes in (a) the H form and (b) the Cs form.

In order to determine the direction of ion transport inside the nanofibers the crystal structure of titanate nanotubes needs to be considered. Although there is much discussion on the exact crystal structure of titanate nanofibers, it is generally agreed that they have a layered structure consisting of parallel planes. Figure 12a shows a HRTEM image of titanate nanofibers in protonated form and demonstrates two different set of fringes. The angle between two sets is ca. 106°, which corresponds to the β angle of monoclinic titanate. The approximate interplanar distances are 0.64 and 0.36 nm; the first value corresponding to the characteristic interlayer spacing d_{200} being intrinsic to all layered titanates.

The ion exchange of protons to Cs^+ ions in titanate nanofibers results in a change of crystallographic β angle to 120° and an increase of d_{200} spacing to 0.83 nm (see Figure 12b) suggesting that a significant transformation of crystal structure occurs. Surprisingly, the XRD pattern of Cs-substituted titanate nanofibers does not show the characteristic (200) reflection (see Figure 13), which is expected at smaller angles. This may be due to systematic extinction of the (200) reflection due to the change of symmetry in the crystal lattice. Indeed, the 120° angle may indicate a higher symmetry in the crystal.

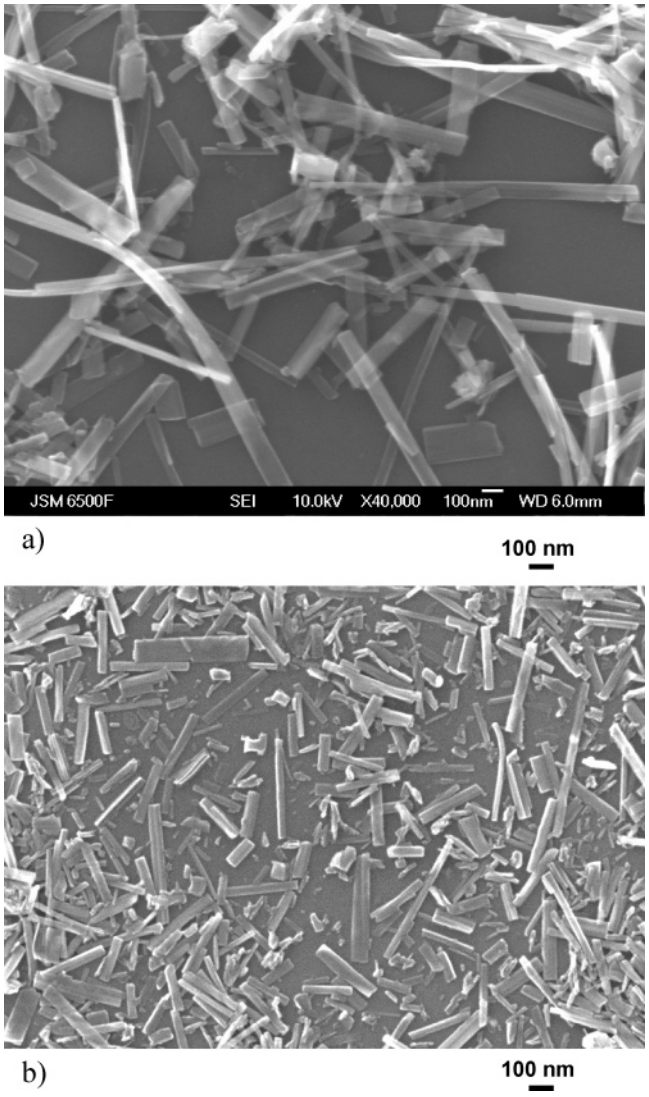

Figure 10. SEM images of titanate nanofibers on a silicon wafer: (a) initial nanofibers and (b) nanofibers treated with ultrasound for 2 h.

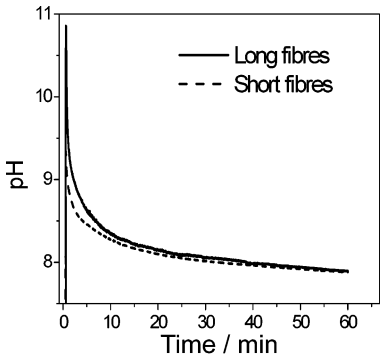

Figure 11. pH decay following addition of 50 μL of 1 mol dm^{-3} LiOH to a suspension of 0.1 g of protonated titanate nanofibers in 10 mL of water at 25 °C. The "long" fibers are an initial sample; the "short" fibers were produced by ultrasonic treatment for 2 h.

Another important observation is the ca. 30% increase of d_{200} spacing due to the intercalation of Cs^+ ions between layers of the titanate. Together with the dependence of intercalation rate

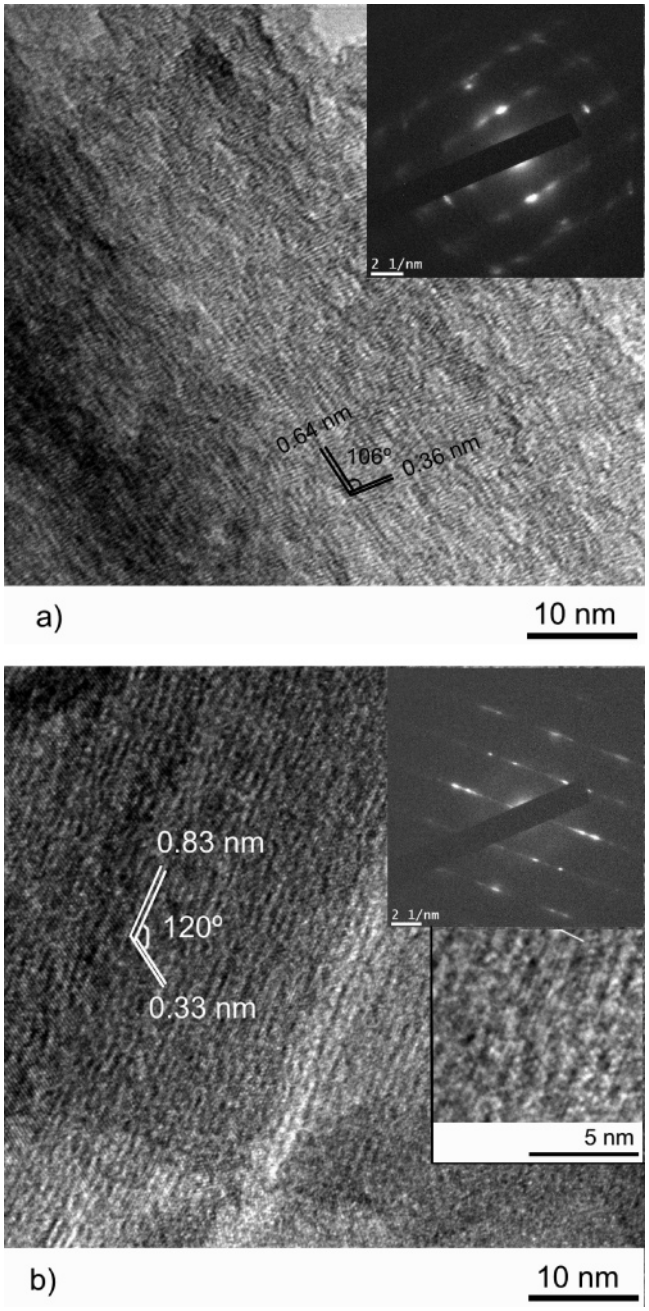

Figure 12. HRTEM images of titanate nanofibers in (a) the protonated form and (b) the Cs form. The insets show SAED images and a high-magnification image of samples.

on the length and thickness of the nanofibers, this may suggest that the transport of ions occurs between, rather than across, the layers of the crystal.

Figure 14 shows the transformation of titanate nanosheets to nanotubes or nanofibers with a consistently oriented crystallographic axis. During the growth of nanosheets, under alkaline hydrothermal conditions, the growth rate in three principal directions follows the order $r_{001} \gg r_{100} \gg r_{010}$.[34] At a certain time, the bending of nanosheets around axis *b* occurs due to the mechanical tensions,[8] or asymmetrical chemical environment[35,36] followed by closing the loop[37] and growth along the direction *b*. If the formation of a nanotube did not occur, the produced nanofibers have a length corresponding the direction *c* and a thickness corresponding to both directions *a* and *b* (see Figure 14). As described above, the transport of cations of alkaline metals in titanate nanotubes occurs preferably along

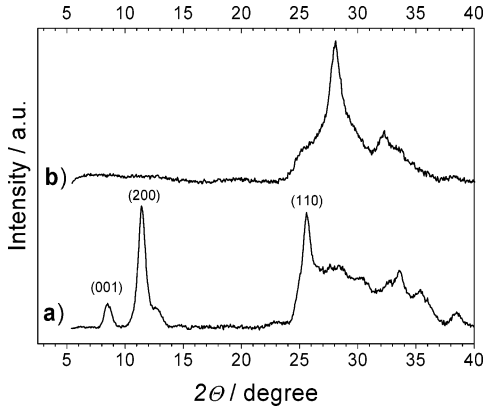

Figure 13. Powder XRD patterns of titanate nanofibers in (a) the H form and (b) the Cs form.

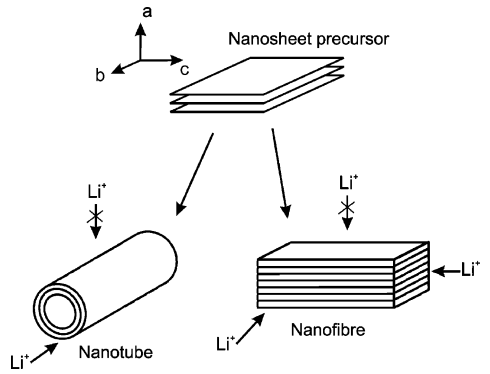

Figure 14. Orientation of crystallographic axes in titanate nanostructures and the directions of cation transport.

the length of nanotubes, which corresponds to the axis *b*. In case of nanofibers, the transport of cations preferably occurs along the axes *b* and *c*. The length of the nanotubes (being around hundreds of nanometers) is of the same order of magnitude as the thickness of nanofibers (along direction *b*). Taking into account that the characteristic time of ion exchange is similar for nanotubes and nanofibers, it is possible to conclude that the transport of ions in nanofibers in direction *b* is dominant.

Conclusions

The kinetics of alkali metal ion intercalation into nanotubular or nanofibrous titanates from an aqueous suspension has been studied. For both nanotubes and nanofibers, the insertion of all alkali ions studied (Li^+, Na^+, K^+, Cs^+) occurs between the layers of crystal resulting in ca. 30% rise the corresponding interplanar distance d_{200}. The rate of intercalation into nanotubes is the same for all the cations, and the limiting stage of the process is likely to be diffusion of ions inside the solid crystal. In the case of nanotubes, the ions probably diffuse along the length of the tube; in the case of nanofibers, ion transport in the direction perpendicular to the length of the fiber is probably dominant. The diffusion coefficient of the lithium cation inside the nanotubes was estimated as an order of magnitude of 10^{-11} $cm^2\ s^{-1}$. The intercalation of alkali metal cations into nanotubes affects only the interlayer spacing d_{200}, whereas, in the case of nanofibers, more significant modification of crystal structures with a possible change of symmetry of lattice occurs, indicating greater structural rigidity in the nanotubes.

Acknowledgment. The authors are grateful to Dr. Barbara Cressey (University of Southampton) for her assistance with the TEM imaging and measurements.

References and Notes

(1) Lu, J. G.; Chang, P.; Fan, Z. *Mater. Sci. Eng.* **2006**, *52*, 49.
(2) Chen, Q.; Peng, L. M. *Int. J. Nanotechnol.* **2007**, *4*, 44.
(3) Bavykin, D. V.; Friedrich, J. M.; Walsh, F. C. *Adv. Mater.* **2006**, *18*, 2807.
(4) Chen, X.; Mao, S. S. *J. Nanosci. Nanotechnol.* **2006**, *6*, 906.
(5) Bavykin, D. V.; Lapkin, A. A.; Plucinski, P. K.; Friedrich, J. M.; Walsh, F. C. *J. Phys. Chem. B* **2005**, *109*, 19422.
(6) Armstrong, A. R.; Armstrong, G.; Canales, J.; Bruce, P. G. *J. Power Sources* **2005**, *146*, 501.
(7) Cheng, F.; Chen, J. *J. Mater. Res.* **2006**, *21*, 2744.
(8) Bavykin, D. V.; Parmon, V. N.; Lapkin, A. A.; Walsh, F. C. *J. Mater. Chem.* **2004**, *14*, 3370.
(9) Sun, X.; Li, Y. *Chem. Eur. J.* **2003**, *9*, 2229.
(10) Girishkumar, G.; Rettker, M.; Underhile, R.; Binz, D.; Vinodgopal, K.; McGinn, P.; Kamat, P. *Langmuir* **2005**, *21*, 8487.
(11) Ali, I. M. *J. Radioanal. Nucl. Chem.* **2004**, *260* (1), 149.
(12) Fan, R.; Yue, M.; Karnik, R.; Majumdar, A.; Yang, P. *Phys. Rev. Lett.* **2005**, *95*, 086607.
(13) Ma, R.; Sasaki, T.; Bando, Y. *Chem. Commun.* **2005**, *7*, 948.
(14) Kasuga, T.; Hiramatsu, M.; Hoson, A.; Sekino, T.; Niihara, K. *Langmuir* **1998**, *14*, 3160.
(15) Li, C.; Zhang, H. P.; Fu, L. J.; Liu, H.; Wu, Y. P.; Ram, E.; Holze, R.; Wu, H. Q. *Electrochim. Acta* **2006**, *51* (19), 3872.
(16) Zhou, Y. K.; Cao, L.; Zhang, F. B.; He, B. L.; Liz, H. L. *J. Electrochem. Soc.* **2003**, *150*, A1246.
(17) Li, J.; Tang, Z.; Zhang, Z. *Electrochem. Commun.* **2005**, *7*, 62.
(18) Kavan, L.; Kalbac, M.; Zukalova, M.; Exnar, I.; Lorenzen, V.; Nesper, R.; Graetzel, M. *Chem. Mater.* **2004**, *16*, 477.
(19) Li, J.; Tang, Z.; Zhang, Z. *Chem. Mater.* **2005**, *17*, 5848.
(20) Chen, Q.; Du, G. H.; Zhang, S.; Peng, L. M. *Acta Crystallogr., Sect. B* **2002**, *58*, 587.
(21) Yang, J. J.; Jin, Z. S.; Wang, X. D.; Li, W.; Zhang, J. W.; Zhang, S. L.; Guo, X. Y.; Zhang, Z. J. *Dalton Trans.* **2003**, *20*, 3898.
(22) Nakahira, A.; Kato, W.; Tamai, M.; Isshiki, T.; Nishio, K.; Aritani, H. *J. Mater. Sci.* **2004**, *39*, 4239.
(23) Armstrong, G.; Armstrong, A. R.; Canales, J.; Bruce, P. G. *Chem. Commun.* **2005**, *19*, 2454.
(24) Yuan, Z. Y.; Su, B. L. *Colloids Surf., A* **2004**, *241*, 173.
(25) Du, G. H.; Chen, Q.; Han, P. D.; Yu, Y.; Peng, L. M. *Phys. Rev. B* **2003**, *67*, 035323.
(26) Bavykin, D. V.; Cressey, B. A.; Walsh, F. C. *Aust. J. Chem.* **2007**, *60*, 95.
(27) Dickenson, T.; Fiennes, A. *Chemical Kinetics*; Pergamon, 1966.
(28) Crank, J. *The Mathematics of Diffusion*; Clarendon Press: Oxford, 1956.
(29) Mon, J.; Deng, Y.; Flury, M.; Harsh, J. B. *Microporous Mesoporous Mater.* **2005**, *86*, 277.
(30) Stenina, I. A.; Aliev, A. D.; Dorhout, P. K.; Yaroslavtsev, A. B. *Inorg. Chem.* **2004**, *43*, 7141.
(31) Lide, D. R., Ed. *CRC Handbook of Chemistry and Physics*, 84th ed.; CRC Press, 2003.
(32) Ferreira, O. P.; Souza-Filho, A. G.; Mendes-Filho, J.; Alves, O. L. *J. Braz. Chem. Soc.* **2006**, *17*, 2, 393.
(33) Bavykin, D. V.; Friedrich, J. M.; Lapkin, A. A.; Walsh, F. C. *Chem. Mater.* **2006**, *18*, 1124.
(34) Yang, H. G.; Zeng, H. C. *J. Am. Chem. Soc.* **2005**, *127*, 270.
(35) Zhang, S.; Peng, L. M.; Chen, Q.; Du, G. H.; Dawson, G.; Zhou, W. Z. *Phys. Rev. Lett.* **2003**, *91* (25), 256103.
(36) Zhang, S.; Chen, Q.; Peng, L. M. *Phys. Rev. B* **2005**, *71*, 014104.
(37) Kukovecz, A.; Hodos, M.; Horvath, E.; Radnoczi, G.; Konya, Z.; Kiricsi, I. *J. Phys. Chem. B* **2005**, *109*, 17781.